

Theoretical Study of the Dynamics of the $\text{HBr}^+ + \text{CO}_2 \rightarrow \text{HOCO}^+ + \text{Br}$ Reaction

Yuheng Luo, Kazuumi Fujioka, Alyson Shoji, William L. Hase, Karl-Michael Weitzel, and Rui Sun*

Cite This: <https://dx.doi.org/10.1021/acs.jpca.0c05323>

Read Online

ACCESS |



Metrics & More

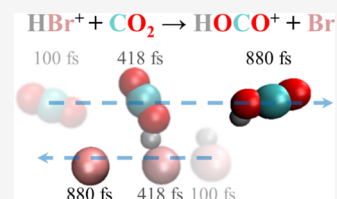


Article Recommendations



Supporting Information

ABSTRACT: The dynamics of the $\text{HBr}^+ + \text{CO}_2 \rightarrow \text{HOCO}^+ + \text{Br}$ reaction was recently investigated with guided ion beam experiments under various excitations (collision energy of the reactants, rotational and spin-orbital states of HBr^+ , etc.), and their impacts were probed through the change of the cross section of the reaction. The potential energy profile of this reaction has also been accurately characterized by high-level *ab initio* methods such as CCSD(T)/CBS, and the UMP2/cc-pVDZ/lanl08d has been identified as an ideal method to study its dynamics. This manuscript reports the first *ab initio* molecular dynamics simulations of this reaction at two different collision energies, 8.1 kcal/mol and 19.6 kcal/mol. The cross sections measured from the simulations agree very well with the experiments measured with HBr^+ in the ${}^2\Pi_{1/2}$ state. The simulations reveal three distinct mechanisms at both collision energies: direct rebound (DR), direct stripping (DS), and indirect (Ind) mechanisms. DS and Ind make up 97% of the total reaction. The dynamics of this reaction is also compared with nucleophilic substitution ($\text{S}_{\text{N}}2$) reactions of $\text{X}^- + \text{CH}_3\text{Y} \rightarrow \text{CH}_3\text{X} + \text{Y}^-$ type. In summary, this research has revealed interesting dynamics of the $\text{HBr}^+ + \text{CO}_2 \rightarrow \text{HOCO}^+ + \text{Br}$ reaction at different collision energies and has laid a solid foundation for using this reaction to probe the impact of rotational excitation of ion-molecule reactions in general.



I. INTRODUCTION

A fundamental understanding of the dynamics of elemental chemical reactions plays an essential role in probing into the mechanisms of more complicated ones.¹ Gas-phase reactions, where the densities of the reactants are extremely low, are ideal systems for studying reaction dynamics and have attracted attention from chemists over a few decades.^{2–4} Recently, Paetow et al.^{5,6} have employed a guided ion beam apparatus to study the dynamics of the proton-transfer reaction of $\text{HBr}^+ + \text{CO}_2 \rightarrow \text{HOCO}^+ + \text{Br}$ under various excitation conditions. Three independent variables were controlled while measuring the cross sections of the reaction: the collision energy between HBr^+ and CO_2 , the rotational energy of HBr^+ , and the angular momentum of HBr^+ (and DBr^+). It is important to note that in their experiments, the HBr^+ ions were specifically prepared at two different spin-orbit (SO) states, ${}^2\Pi_{3/2}$ and ${}^2\Pi_{1/2}$, to study the impact of the SO effect as well as the thermal effect on the dynamics of the reaction, since the difference in the potential energy between the two SO states would change the reaction from slightly endothermic (${}^2\Pi_{3/2}$) to slightly exothermic (${}^2\Pi_{1/2}$).

For the endothermic reaction (i.e., HBr^+ in the ${}^2\Pi_{3/2}$ SO state), Paetow et al.^{5,6} have discovered that the cross section of the reaction increases with the collision energy at all rotational energy levels of the ion (from 1.4 to 66.3 meV). When the collision energy is fixed, an increase in the rotational energy of HBr^+ also reduces the cross section and this effect is more significant at the higher collision energies (i.e., larger than 0.85 eV). For the exothermic reaction (i.e., HBr^+ in the ${}^2\Pi_{1/2}$ SO state), increasing the collision energy actually inhibits the

reaction. The impact of the rotational excitation of HBr^+ (from 3.4 to 46.8 meV) is more complicated for the exothermic reaction: the cross section is largely independent of the rotation of the ion at high (larger than 1.50 eV) collision energies but demonstrates a negative correlation to the rotational excitation at intermediate (between 0.25 and 1.50 eV) collision energies. When the collision energy is low (less than 0.25 eV), as the rotational energy of HBr^+ increases, the cross section first decreases, reaches a minimum, and then increases again. In a later paper, Uhlemann et al.⁷ explained a similar minimum in the cross section of the $\text{HCl}^+ + \text{HCl}$ reaction by a model comparing the rotational velocity of the ion to that of the neutral. These phenomena, especially that of the rotational excitation, could not be simply explained by the potential energy profile of the reaction (endothermic vs exothermic), indicating that some complicated mechanism might have taken place.

Quantum chemistry calculation has been an effective method of studying the energy profile of gas-phase reaction since its development in the early 1950s.^{8,9} There have been several *ab initio* calculations to unravel the potential energy profile of the reaction, including the original manuscript of

Received: June 11, 2020

Revised: October 9, 2020

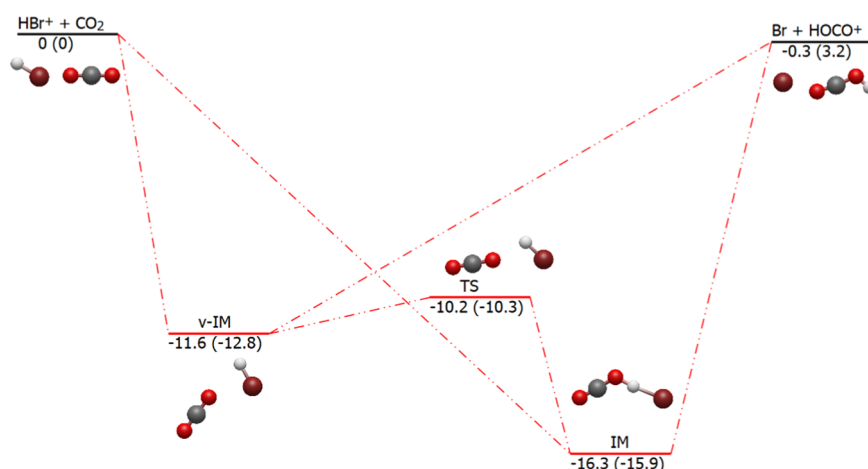


Figure 1. Potential energy profile of the $\text{HBr}^+ + \text{CO}_2 \rightarrow \text{HOCO}^+ + \text{Br}$ reaction. The values are calculated with the UMP2/cc-pVDZ/lanl08d level of theory, and the values in parentheses are calculated with CCSD(T)/CBS.¹¹ Both values (in kcal/mol) are without zero-point energy and spin-orbit coupling effect.

Paetow et al.,⁵ in which the relative potential energies of the products and the hydrogen bond intermediate, IM ($[\text{BrH}\cdots\text{OCO}]^+$), were calculated with CCSD(T)/TZ2P from the structures optimized with MP2/TZ2P. Later, Sun et al.¹⁰ studied the potential energy profile of this reaction with the CCSD(T) geometry optimization and reported another van der Waals intermediate ($[\text{HBr}\cdots\text{OCO}]^+$), v-IM, which lies about 0.13 eV above the IM. Recently, Shoji et al.¹¹ have identified a transition state (TS) that connects the aforementioned IM and v-IM. The potential energy profile of the reaction suggests that as the reactant molecules approach each other, depending on their relative orientation, either one of the two intermediates could form. These intermediates could interconvert into each other by crossing the low TS (barrier height less than 0.25 eV) between them before eventually dissociating into products.^{12–14}

It is well known that the potential energy profile alone provides only a steady-state picture of the chemical reaction, and the information derived from the energy profile (e.g., reaction rate, time-of-flight of the product, etc.) is only true under the assumption that a statistical ensemble is maintained for all intermediates involved,^{12,15,16} i.e., the lifetime of the intermediates formed after the collision is sufficient for the intramolecular vibrational redistribution (IVR). In addition, the knowledge of the potential energy profile alone does not guarantee understanding the full reaction dynamics, as many ion–molecule reactions have been reported to contain a significant portion of direct reaction (without forming intermediates), barrier recrossings, and other non-IRC behaviors.^{17–19}

Ab initio molecular dynamics (AIMD) simulations^{2,20} have been employed to unravel complicated and nonintuitive reaction dynamics by following the motion of atoms in real time. In AIMD, a large number of trajectories that represent the physical ensemble of the reactants are simulated and the trajectories are updated iteratively according to classical equations of motion with the forces computed from quantum calculations. Herein, a few thousand AIMD trajectories of this reaction with a low (0.35 eV, 8.1 kcal/mol) and medium (0.85 eV, 19.6 kcal/mol) collision energy are simulated with no rotational excitation of HBr^+ . The cross section computed from AIMD simulations shows excellent agreement with the exothermic reaction (HBr^+ in the $^2\Pi_{1/2}$ SO state), and the

trajectories have revealed several interesting characteristics of the reaction dynamics. This study has laid a solid foundation for future investigation on how the rotational excitation impacts the dynamics of the reaction.

This article is organized as follows: The potential energy profile of the reaction and the details of AIMD simulations are briefly introduced in the **Methods** section. The Results section reports the dynamics of the reaction, including the reaction probability, the reaction mechanism, the scattering angle of the reaction, and the partitioning of the kinetic energy in the product. This article concludes with a comparison between the AIMD simulations and the experiments and a discussion of where the dynamics of this reaction is different from other common ion–molecule reactions.

II. METHODS

II.1. Potential Energy Surface. As stated in the previous section, the potential energy profile (shown in **Figure 1**) of the $\text{HBr}^+ + \text{CO}_2 \rightarrow \text{HOCO}^+ + \text{Br}$ reaction has been characterized by Sun et al.¹⁰ and Shoji et al.¹¹ In Sun et al.,¹⁰ the potential energy profile, including the reaction energy, the H-bonded intermediates (IM), and the van der Waals intermediates (v-IM), is characterized by the coupled cluster theory with complete basis set limit (CCSD(T)²¹/CBS^{22,23}). In a more recent study by Shoji et al.,¹¹ a transition state (TS) that connects the aforementioned intermediates has been identified at a similar level of theory, making the reaction potential energy profile double-welled. Frankly, CCSD(T) is infeasible for AIMD simulations and Shoji et al.¹¹ have systematically screened various inexpensive quantum mechanics methods (e.g., different combinations of single reference methods such as density functional theory (DFT)²⁴ functionals and MP2,²⁵ basis sets,²⁶ and effective core potentials²⁷ on Br) and suggested employing UMP2²⁵/cc-pVDZ²⁸/lanl08d²⁹ for AIMD simulations due to its optimal accuracy/cost ratio. The energy profile computed with UMP2/cc-pVDZ/lanl08d and its comparison to the benchmark energy from CCSD(T)/CBS are depicted in **Figure 1**.

It is important to note that the UMP2/cc-pVDZ/lanl08d employed in this AIMD study is not able to explicitly account for the SO coupling effect, and as a result, the AIMD trajectories are considered to operate on a “spin-averaged”

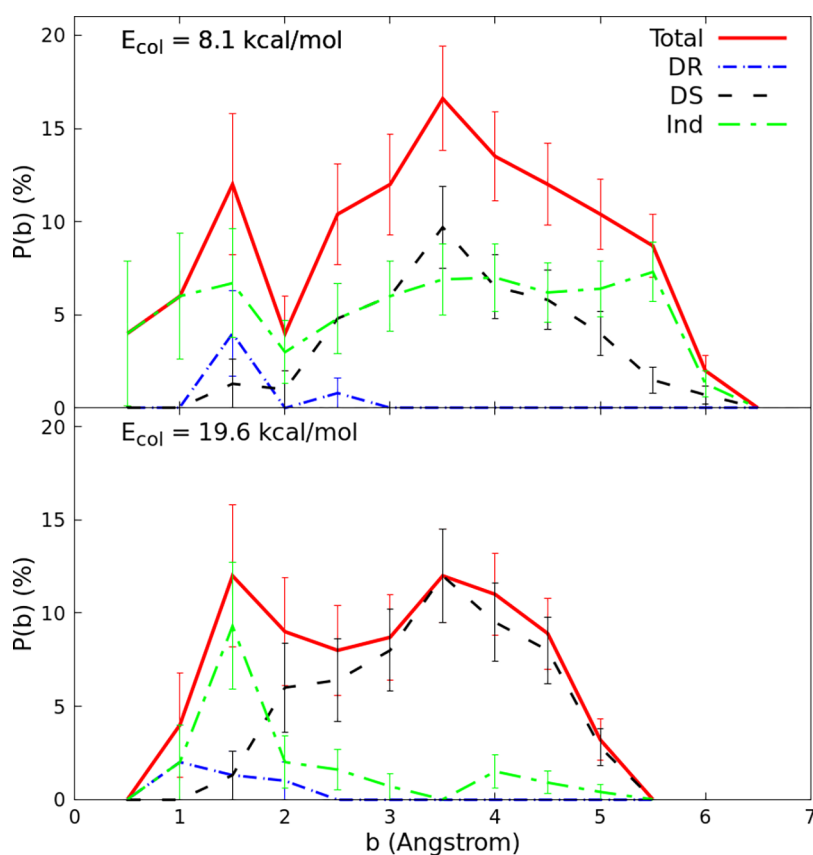


Figure 2. The reaction probability, $\rho(b)$, vs the impact parameter, b , from the AIMD simulations.

state between the two. This choice clearly compromises the ability of AIMD to distinguish the difference in the reaction dynamics introduced by the SO effect but is deemed to be necessary for the following reasons: first and foremost, this compromise is a result of the excessive amount of energy gradient calculations demanded by the AIMD simulation (about 28 million, details explained in the next section). An accurate account of the SO coupling effect on-the-fly would require some multireference *ab initio* method such as state-averaged complete active space self-consistent field (SA-CASSCF)³⁰ and the computation cost of millions of such energy gradient calculations would be infeasible. Further, for HBr⁺, a Π state diatomic molecule with one unpaired electron, the addition and subtraction between the orbital and the spin angular momenta result in two SO coupling states, $\pm 3/2$ ($^2\Pi_{3/2}$, ground state) and $\pm 1/2$ ($^2\Pi_{1/2}$), respectively. These SO states are separated by 328 meV (7.6 kcal/mol), and the average of these SO coupling states lies in the middle (i.e., 3.8 kcal/mol above the $^2\Pi_{3/2}$ state and 3.8 kcal/mol below the $^2\Pi_{1/2}$ state). As a result, simply from the perspective of the total energy of the reaction, the “spin-averaged” potential energy from the UMP2/cc-pVDZ/lanl08d adds 3.8 kcal/mol to the $^2\Pi_{3/2}$ state and subtracts 3.8 kcal/mol from the $^2\Pi_{1/2}$ state.¹¹ We acknowledge that the SO coupling effect could have a more complicated impact on the dynamics than merely an additional term of energy; nevertheless, Sun et al.¹⁰ have demonstrated that the SO coupling changes smoothly from the reactants to the products with a comprehensive geometry scan (e.g., the SO coupling energy is computed at thousands of configurations that could be populated in the phase space throughout the reaction). The hypothesis of the SO coupling

effect being mainly an effect of additional energy is in fact also supported by the results of Paetow et al.,^{5,6} which demonstrates that the main effect of going from one spin-orbit state to the other is to change the effective reaction enthalpy from endothermic for the SO ground state to exothermic for the excited SO state. Therefore, the main difference in the cross sections measured pertains to the collision energy dependence being characteristic for endothermic and exothermic reactions. As a result, for the present research, the spin-free UMP2/cc-pVDZ/lanl08d level of theory is considered to be acceptable in probing the dynamics of this reaction.

II.II. AIMD Simulations. The AIMD simulations are set to model the conditions of the guided ion beam experiment as close as possible. The two reactant molecules, HBr⁺ and CO₂, are initially separated by 12 Å (center-of-mass distance), far enough that the interaction between them is negligible. The relative orientation between these two linear molecules is randomly sampled. HBr⁺ and CO₂ are set to collide with a fixed relative translational energy of either 8.1 kcal/mol (0.35 eV) or 19.6 kcal/mol (0.85 eV). This translational energy is distributed into both reactant molecules, while the total momentum of the system is zero. The initial vibrational and rotational energies for CO₂ are selected from a canonical ensemble at room temperature (298.15 K), while the vibrational and rotational quantum numbers of HBr⁺ are set to zero to approximate the vibration and rotation of its experimental conditions.^{5,6} The position of the atoms is propagated by VENUS³¹ using the velocity Verlet algorithm with the energy gradients calculated from UMP2/cc-pVDZ/lanl08d in NWChem.^{32,33} Most of the AIMD trajectories adopt

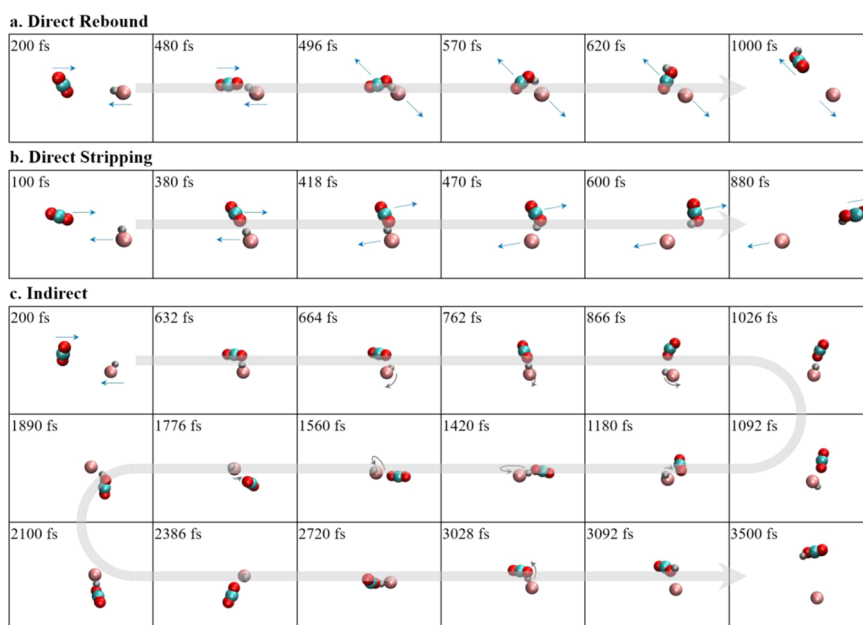


Figure 3. Snapshots of three representative trajectories from different reaction mechanisms. The blue arrows denote the relative translation of the molecules and the gray arrows denote the relative rotation. The blue arrows in the last frame of Ind are omitted to emphasize that the scattering angle of Ind is isotropic. The bond gray arrow represents the time evolution.

a 0.2 femtosecond time step, the largest time step that conserves the total energy of the system. The time step is subjected to decrease to as low as 0.05 femtosecond for some of the unstable trajectories. The trajectories are halted once the products are clearly formed (i.e., the center-of-mass distance between HOCO^+ and Br exceeds 12 Å) or they return to the reactants (i.e., the center-of-mass distance between HBr^+ and CO_2 exceeds 12 Å).

The AIMD simulations need to sample a large enough number of trajectories that represent the physical ensemble of the guided ion beam experiment to capture the dynamics of the reaction. For each collision energy, the largest impact parameter, b_{max} , is detected by systematically increasing the impact parameter b , starting from 4.0 Å with an increment of $\Delta b = 0.5$ Å. At each impact parameter, 50 trajectories are sampled and b_{max} is identified as the largest b where at least one trajectory is reactive. In the production run, trajectories are only calculated with $b < b_{\text{max}}$ and the number of trajectories sampled at each impact parameter is proportional to the impact parameter (see the Supporting Information for justification), starting with 25 trajectories at the smallest impact parameter of $b_{\text{min}} = 0.5$ Å.³⁴ Therefore, the number of trajectories sampled at each b , $N(b)$, is computed as

$$N(b) = N(b_{\text{min}}) \cdot \frac{b}{b_{\text{min}}}; \quad b \leq b_{\text{max}} \quad (1)$$

Depending on their initial conditions, different trajectories experience different lifetimes. For $E_{\text{col}} = 8.1$ kcal/mol, the longest, shortest, and average integration times are 10.6, 1.1, and 2.0 ps, respectively; for $E_{\text{col}} = 19.6$ kcal/mol, the longest, shortest, and average trajectory integration times are 7.4, 0.8, and 1.1 ps, respectively. The total number of AIMD trajectories is 3425, and the total number of UMP2/cc-pVDZ/lanl08d energy gradient calculations exceeds 28 million. Ninety-seven percent of total trajectories have less than 0.1 kcal/mol of energy conservation error. The average energy conservation error for both collision energies is 0.04 kcal/mol.

The largest energy conservation error is 0.4 kcal/mol for $E_{\text{col}} = 8.1$ kcal/mol and 0.8 kcal/mol for $E_{\text{col}} = 19.6$ kcal/mol. The average and maximum eigenvalues of the total spin-squared operator during the trajectories are 0.759 and 0.777, respectively.

III. RESULTS

III.I. Overview of the Reaction Mechanisms. The reaction probability ($\rho(b)$) vs impact parameters (b) are shown as a red curve in Figure 2. This figure is derived from the summary of the simulation in the Supporting Information (Table S1). Reactions of both collision energies show a similar trend: Starting from $b = 0.5$ Å, $\rho(b)$ increases as b increases. Beyond a local maximum at $b = 1.5$ Å, $\rho(b)$ shows a significant dip at 2.0 Å ($E_{\text{col}} = 8.1$ kcal/mol) and 2.5 Å ($E_{\text{col}} = 19.6$ kcal/mol). Thereafter, $\rho(b)$ increases again with the increase of b , reaching the largest reaction probability at $b = 3.5$ Å. Further increase of b from $b = 3.5$ Å decreases $\rho(b)$. The b_{max} for $E_{\text{col}} = 8.1$ kcal/mol, 6.0 Å, is 1.0 Å larger than that of $E_{\text{col}} = 19.6$ kcal/mol. At large b values, instead of colliding directly (i.e., “head-to-head”), the two reactant molecules are figuratively “passing by” each other. Combining the difference in the nature of the collision induced by impact parameter with the fact that the higher the E_{col} , the faster the relative velocity between HBr^+ and CO_2 , there is less time for the two reactant molecules to interact with each other at high E_{col} and large b , diminishing the chances for reaction.

AIMD trajectories of both collision energies have revealed three distinct mechanisms of the reaction: direct rebound (DR), direct stripping (DS), and indirect (Ind). Snapshots from a representative DR mechanism are shown in Figure 3a. In DR, the HBr^+ ion collides with the CO_2 molecule “head-to-head” while pointing the proton toward the CO_2 . The proton transfers from the HBr^+ to the oxygen of the CO_2 and forms an HOCO^+ ion, which immediately bounces off of the massive Br . Snapshots from a representative DS mechanism are shown in Figure 3b: the proton is still pointed toward the colliding

center, while the HBr^+ ion touches CO_2 from its terminal (i.e., one of the oxygens) and loses the proton. The newly formed HOCO^+ ion immediately leaves Br without getting trapped in either of the intermediates (i.e., IM or v-IM). In contrast to DR and DS, the Ind mechanism includes all trajectories that show a detectable lifetime of the intermediates and/or transitions between them. An example set of the snapshots of the Ind trajectories is depicted in Figure 3c. Due to the excess energy available in the system, the intermediate formed after collision is highly vibrationally and rotationally excited and the system is transiting between the two intermediates multiple times before eventually dissociating into products. One representative animation of the trajectory for each reaction mechanism can be found in the Supporting Information.

III.II. Correlation between Impact Parameter (b) and Reaction Mechanism. Figure 2 shows that the aforementioned reaction mechanisms are highly correlated with the impact parameter. As stated in the previous section, the DR mechanism demands a head-to-head collision; thus, it only appears at low b values (i.e., $b \leq 2.5$ Å) for both collision energies (blue dot-dashed curve in Figure 2). In contrast, the DS mechanism is triggered by HBr^+ attacking the oxygen of the CO_2 molecule (i.e., offloading the proton to it) at a relatively large distance. As a result, DS trajectories are only observed for $b \geq 1.5$ Å and they are predominantly observed at large b values (black dashed curve in Figure 2). In contrast, the Ind mechanisms only require the formation of intermediates and thus are observed in all b values.

It is important to note that collision energy could have a profound impact on the reaction mechanisms. The two direct mechanisms are somewhat independent of the collision energy: DR is only observed at very low b values and DS predominates at large b . Aligning with the trend of the total reaction probability, the reaction probability of DR (ρ_{DR}) and DS (ρ_{DS}) both decreases when collision energy increases, and the ratio between them (i.e., $\rho_{\text{DR}}/\rho_{\text{DS}}$) remains similar: 0.05 for $E_{\text{col}} = 8.1$ kcal/mol vs 0.03 for $E_{\text{col}} = 19.6$ kcal/mol. As shown in Figure 2, the collision energy has a much larger impact on the probability of the Ind mechanism (ρ_{Ind}): at $E_{\text{col}} = 8.1$ kcal/mol, ρ_{Ind} is almost independent of impact parameters in the range of $1.0 \text{ Å} \leq b \leq 5.5 \text{ Å}$; however, the Ind trajectories of $b \geq 2.0$ Å are largely absent at $E_{\text{col}} = 19.6$ kcal/mol. This phenomenon can be attributed to the slow approach of the reactants at low collision energy, allowing abundant time for intermolecular interactions between HBr^+ and CO_2 to form intermediates even at large b values. In the case of high collision energy, the time window that allows for the two reactant molecules to interact and form an intermediate is too short; consequently, the two molecules have a higher chance of just flying by each other.

Among the three reaction mechanisms, DR makes up less than 3% of the total reactive trajectories and makes an insignificant contribution to the total reaction probability (see Figure 2). Ind is the predominant reaction mechanism at low impact parameters and accounts for 57 and 17% of the total reactive trajectories for $E_{\text{col}} = 8.1$ kcal/mol and $E_{\text{col}} = 19.6$ kcal/mol, respectively. More than 80% of the total reactive trajectories for $E_{\text{col}} = 19.6$ kcal/mol are DS, and they are largely observed at $b \geq 2.0$ Å. The analysis of the reaction mechanism at different impact parameters unravels the mysterious dip at the medium impact parameter ($b = 2.0$ Å for $E_{\text{col}} = 8.1$ kcal/mol and $b = 2.5$ Å for $E_{\text{col}} = 19.6$ kcal/mol), and the reasons

are different for the two collision energies. For $E_{\text{col}} = 8.1$ kcal/mol, the dip is a result of two concerted efforts: the fast decrease of DR and the absence of DS at $b = 2.0$ Å; for $E_{\text{col}} = 19.6$ kcal/mol, the dip is mostly due to the sudden decline of the probability for Ind for the reason mentioned in the previous paragraph.

III.III. Scattering Angle and Energy Partitioning in the Products. The reaction mechanisms have been reported to have a profound impact on the dynamics of the product for ion–molecule reactions. The AIMD simulations of the $\text{HBr}^+ + \text{CO}_2 \rightarrow \text{HOCO}^+ + \text{Br}$ reaction have demonstrated a similar trend. The scattering angle of this reaction is defined as the angle (θ) between the velocities of the incoming ion, HBr^+ , and the leaving atom, Br. Figure 4 shows that the θ from the

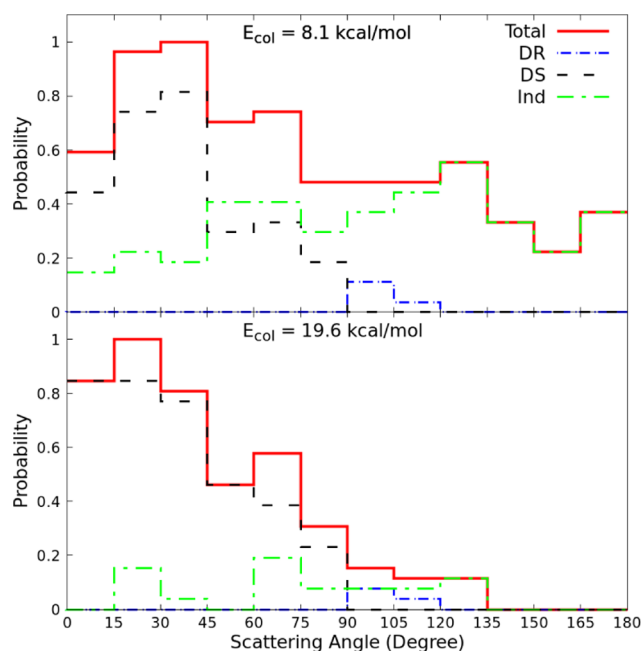


Figure 4. Scattering angle (defined in the text) distribution from the AIMD simulations. The maximum probability is set to 1.

DR trajectories are obtuse (backward scattering, 107 ± 8 and $100 \pm 8^\circ$ for $E_{\text{col}} = 8.1$ kcal/mol and $E_{\text{col}} = 19.6$ kcal/mol, respectively) since in DR, the HBr^+ collides (at small impact parameter) into the CO_2 , transfers a proton, and has the remaining Br atom bouncing off in the backward direction. As a result of this head-to-head collision, the compounds (defined as HBr^+/Br and $\text{CO}_2/\text{HOCO}^+$) approximately exchange the direction of their velocities, e.g., Br is moving in the opposite direction as the direction of HBr^+ before the collision, leading to an obtuse angle. The DS trajectories are associated with acute θ (forward scattering, shown in Figure 4), i.e., 36 ± 22 and $34 \pm 23^\circ$ for $E_{\text{col}} = 8.1$ kcal/mol and $E_{\text{col}} = 19.6$ kcal/mol, respectively. In DS, the HBr^+ moves toward the CO_2 , colliding from the side (at large impact parameter) instead of head-to-head, and offloads the proton. As a result, the directions of the motions of both compounds remain largely unperturbed—Br moves in a similar direction as HBr^+ , resulting in an acute scattering angle. The distribution of θ in the Ind mechanism is much more isotropic than in DR and DS. Since the lifetime of the system trapped in the intermediates after the collision is longer than their IVR, the system will become more uniformly excited before it can dissociate. As a result, the dissociation

becomes a random event and makes the direction of the leaving Br uniformly distributed. The overall scattering angle (red solid curve in Figure 4) of the reaction changed from slightly forward to overwhelmingly forward when the collision energy increased from 8.1 to 19.6 kcal/mol, largely due to the absence of Ind mechanism at the higher collision energy.

Another aspect of the dynamics of the reaction pertains to the partitioning of kinetic energy over the products. Here, the term kinetic energy of the system is the summation of the kinetic energy of each individual atom (i.e., $1/2m_i v_i^2$, i is the index of the atom). A quantitative measurement is carried out by separating the kinetic energy of the system into three categories: (1) the relative translational energy between the products (HOCO^+ and Br), E_{rel} ; (2) the rotational energy of the products (in this reaction, only HOCO^+), E_{rot} ; and (3) the kinetic component of the vibrational energy of the products (in this reaction, only HOCO^+), E_{vib} . The method of computing such energies follows the protocol of classical mechanics and is provided in the Supporting Information. The results of the fractions of E_{rel} , E_{rot} , E_{vib} , and E_{int} (internal energy, i.e., $E_{\text{rot}} + E_{\text{vib}}$) with respect to the total kinetic energy are summarized in Table 1.

Table 1. Kinetic Energy Partitioning of the Products of the $\text{HBr}^+ + \text{CO}_2 \rightarrow \text{HOCO}^+ + \text{Br}$ Reaction^a

	$E_{\text{col}} = 8.1$ kcal/mol			
	f_{rot}	f_{vib}	f_{rel}	f_{int}
DR	0.16 ± 0.18	0.44 ± 0.25	0.40 ± 0.25	0.60 ± 0.25
DS	0.21 ± 0.05	0.34 ± 0.05	0.45 ± 0.06	0.55 ± 0.06
Ind	0.19 ± 0.04	0.37 ± 0.05	0.44 ± 0.05	0.56 ± 0.05
total	0.20 ± 0.03	0.36 ± 0.04	0.44 ± 0.04	0.56 ± 0.04
	$E_{\text{col}} = 19.6$ kcal/mol			
	f_{rot}	f_{vib}	f_{rel}	f_{int}
DR	0.25 ± 0.25	0.41 ± 0.28	0.34 ± 0.27	0.66 ± 0.27
DS	0.16 ± 0.04	0.25 ± 0.05	0.59 ± 0.05	0.41 ± 0.05
Ind	0.31 ± 0.11	0.37 ± 0.11	0.32 ± 0.11	0.68 ± 0.11
total	0.19 ± 0.04	0.28 ± 0.04	0.53 ± 0.05	0.47 ± 0.05

^aThe subscript (rot, vib, rel, and int) denotes the fraction of the rotational, vibrational (kinetic component), relative translational, and internal (rotational + vibrational) energies of the product, respectively.

Since the reaction probability of the DR mechanism is much lower compared to that of DS and Ind (see Figure 2), the error bar associated with its energy partitioning is too large to have statistical significance. Therefore, the focus of the analysis is to compare the impact of the collision energy on the energy partitioning between DS and Ind mechanisms. For $E_{\text{col}} = 8.1$ kcal/mol, the energy partitioning of DS and Ind trajectories is indistinguishable and the E_{int} and E_{rel} are almost equally partitioned (55 vs 45%). In contrast, the DS mechanism at $E_{\text{col}} = 19.6$ kcal/mol has clearly demonstrated its tendency to preserve the relative translation of the system (E_{rel} makes up almost 60% of the total kinetic energy). This result is expected: the higher the collision energy, the less time available for the two molecules to interact with each other. Therefore, the collision should be more elastic, which in turn preserves more relative translational energy. Compared to $E_{\text{col}} = 8.1$ kcal/mol, E_{rel} only makes up one-third of the total kinetic energy in the Ind trajectories at $E_{\text{col}} = 19.6$ kcal/mol. The significant decrease (i.e., from 44 to 33%) in E_{rel} at the higher collision

energy is counterintuitive: as the total energy of the system increases, the Ind trajectories spend less time (on average) being trapped by the two intermediates (0.80 ps vs 0.46 ps for $E_{\text{col}} = 8.1$ kcal/mol and $E_{\text{col}} = 19.6$ kcal/mol, respectively) and the collision should have become more elastic (i.e., preserving more relative transition energy). In addition, upon increasing E_{col} from 8.1 to 19.6 kcal/mol, the loss in fraction of the relative translational energy is all transferred to the rotation of HOCO^+ and the fraction of E_{vib} remains constant. Further discussion of this counterintuitive phenomenon can be found in the next section.

IV. DISCUSSIONS

IV.I. Comparison with Experiments. Paetow et al.^{5,6} have reported the cross sections of the $\text{HBr}^+ + \text{CO}_2 \rightarrow \text{HOCO}^+ + \text{Br}$ reaction under various excitations, and it is of interest to compare them with the AIMD simulations. In regard to the heat of reaction, the reaction is endothermic (experimental reaction energy + 4.8 kcal/mol) if HBr^+ is in the $^2\Pi_{3/2}$ SO state but exothermic (experimental reaction energy -2.6 kcal/mol) if HBr^+ is in the $^2\Pi_{1/2}$ SO state.¹⁰ For the reasons discussed in the Introduction section, the AIMD simulations in this research are performed with a spin-free *ab initio* method (i.e., UMP2/cc-pVDZ/lanl08d). The potential energy profile of this method suggests that the reaction is almost thermoneutral (-0.3 kcal/mol), much closer to the exothermic reaction (HBr^+ in the $^2\Pi_{1/2}$ SO state). The cross section (σ) from AIMD is computed with the following integral

$$\sigma = \int_{b_{\text{min}}}^{b_{\text{max}}} 2\pi b \cdot \rho(b) \cdot db \quad (2)$$

$\rho(b)$ is the reaction probability (see Figure 2) at impact parameter b . The cross sections from AIMD computed with eq 2 are 11.7 ± 2.6 and $7.2 \pm 1.8 \text{ \AA}^2$ for $E_{\text{col}} = 8.1$ kcal/mol and $E_{\text{col}} = 19.6$ kcal/mol, respectively. These values agree well with the experimental cross sections of the exothermic reaction (i.e., HBr^+ in the $^2\Pi_{1/2}$ SO state): 11.7 and $4.8 \pm 0.4 \text{ \AA}^2$ for $E_{\text{col}} = 8.1$ kcal/mol and $E_{\text{col}} = 19.6$ kcal/mol, respectively. It is important to note that the experimental cross section for $E_{\text{col}} = 8.1$ kcal/mol was not directly measured by Paetow et al.^{5,6} (thus does not have an error bar) but interpolated from other cross sections of similar collision energies. In comparison, the cross sections measured from the endothermic reaction (i.e., HBr^+ in the $^2\Pi_{3/2}$ SO state) are much smaller: 1.4 ± 0.3 and $3.3 \pm 0.2 \text{ \AA}^2$ for $E_{\text{col}} = 8.1$ kcal/mol and $E_{\text{col}} = 19.6$ kcal/mol, respectively. The normalized cross sections from the AIMD and the crossed beam experiments of both SO states are summarized in Figure 5. The figure demonstrates that for the exothermic reaction, the cross section decreases with the increase of E_{col} ; for the endothermic reaction, the trend is reversed. Recall that the heat of the reaction according to UMP2/cc-pVDZ/lanl08d is much closer to the exothermic reaction than to the endothermic reaction—it is interesting to note that the AIMD simulations also more accurately represent the dynamics of the former. As a result, further investigation of the impact of the rotational excitation with the UMP2/cc-pVDZ/lanl08d AIMD simulation will be compared with the exothermic reaction only.

IV.II. Comparison with Other Ion–Molecule Reactions. Ion–molecule reactions have been investigated extensively with guided ion beam experiments and AIMD

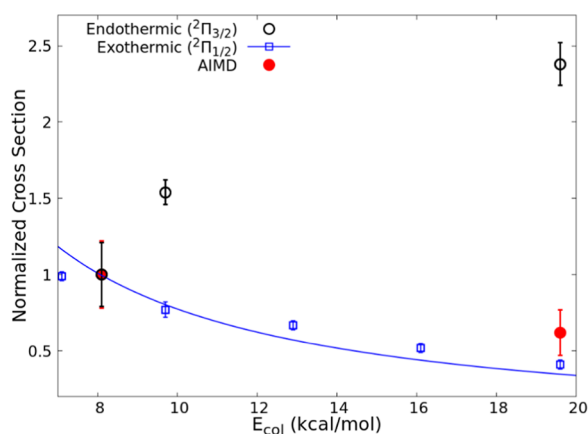


Figure 5. Normalized cross sections from the AIMD simulations and the experiments.^{5,6} The cross sections of $E_{\text{col}} = 8.1$ kcal/mol for both the endothermic and the exothermic are scaled to 1. The blue line is the spline fit of the experimental result of the exothermic reaction.

simulations over the past decade. The dynamics of the nucleophilic substitution ($S_{\text{N}}2$) reactions^{13,35–37} of type $X^- + \text{CH}_3Y \rightarrow \text{CH}_3X + Y^-$ has been selected to compare with the $\text{HBr}^+ + \text{CO}_2 \rightarrow \text{HOCO}^+ + \text{Br}$ reaction for two reasons: (1) both reactions have reported similar mechanisms (i.e., DR, DS, and Ind) and (2) the potential energy profiles of both reactions are double-welled, consisting of a prereaction complex, TS, and postreaction complex. The dynamics of the reaction is probed through three observables: the cross section (σ), the scattering angle (θ), and the energy partitioning of the Ind ($f_{\text{rel}}(\text{Ind})$).

The results of the cross section measured from AIMD of a few $S_{\text{N}}2$ reactions are summarized in Table 2. It should be noted that in addition to the nature of the reaction and the collision energies, the cross section depends heavily on the quantum chemical method that is employed in the AIMD simulation. Take the reaction of $\text{F}^- + \text{CH}_3\text{I} \rightarrow \text{CH}_3\text{F} + \text{I}^-$ as an example: this reaction was first studied with a DFT method, B97-1/aug-cc-pVDZ (with ECP/d on I), because its calculated reaction energy agreed well with experimental results.³⁸ The DFT simulations show good agreement with experiments of low collision energy but were not able to reproduce the scattering angle of the experiment of high collision energy.³⁹ Therefore, the potential energy of the reaction was revisited and MP2/aug-cc-pvdz (with ECP/d on I) was employed for a new set of AIMD simulations.³⁶ Compared to the previous

DFT method, MP2/aug-cc-pvdz is a little worse in representing reaction energy (experimental: -196.8 kJ/mol, B97-1/aug-cc-pVDZ: -195.4 kJ/mol, MP2/aug-cc-pvdz: -177.3 kJ/mol); however, in addition to the traditional Walden inversion (C_{3v}) pathway, it includes a reaction pathway that involves a hydrogen bond complex $[\text{F} \cdots \text{HCH}_2\text{I}]^-$, which is confirmed by high-level CCSD(T) but absent in the potential energy of DFT.⁴⁰ The MP2 simulations show much better agreement with experiments of high collision energy, although it has a much smaller cross section (B97-1/aug-cc-pVDZ: $8.6 \pm 2.2 \text{ \AA}^2$, MP2/aug-cc-pvdz: $1.8 \pm 0.3 \text{ \AA}^2$).³⁶ The smaller cross section is a concerted result of a smaller b_{max} (B97-1/aug-cc-pVDZ: 5.75 \AA , MP2/aug-cc-pvdz: 4.75 \AA) and smaller probability reaction at each impact parameter (B97-1/aug-cc-pVDZ: $\sim 8\%$, MP2/aug-cc-pvdz: $\sim 4\%$). A similar result has been found in the $\text{Cl}^- + \text{CH}_3\text{I} \rightarrow \text{CH}_3\text{Cl} + \text{I}^-$ reaction, where the cross section from BhandH⁴¹ (a DFT functional) is much larger compared to the cross section from MP2.³⁷ The dispersion correction is applied in neither of the simulations. Therefore, the relative difference between the cross sections of different collision energies is more important than the values of the cross section themselves. Table 2 suggests that the cross section of various $S_{\text{N}}2$ reactions decreases when the collision energy increases—a similar trend has been reported for the $\text{HBr}^+ + \text{CO}_2$ reaction. However, it is important to note that unlike the nearly thermoneutral $\text{HBr}^+ + \text{CO}_2$ reaction, all of the $S_{\text{N}}2$ reactions in Table 2 are much more exothermic (E_{rxn} in Table 2). Therefore, there appears to be a general trend that an increment in the collision energy suppresses the cross section of the ion–molecular reaction. According to eq 2, the cross section of a reaction is determined by the reaction probability (ρ) as well as the largest impact parameter that a reaction can be observed (b_{max}), and the increment in collision energy suppresses both (Figure 2 and Table 2, respectively). In the previous section of the manuscript, the suppression of the cross section as a result of the high collision energy has been attributed to inadequate time for the reactant molecule to interact with each other. This statement should hold true in general for all of the product pathways that are energetically accessible, making the collision energy the overwhelmingly predominant factor regardless of the thermal effects (i.e., heat of reaction) of the reaction. It is of interest to further investigate to what extent this general trend applies to.

Table 2. Comparison of the Cross Section (σ), the Largest Impact Parameters (b_{max}), and the Relative Translational Energy of the Ind Mechanism ($f_{\text{rel}}(\text{Ind})$) between the $\text{HBr}^+ + \text{CO}_2 \rightarrow \text{HOCO}^+ + \text{Br}$ Reaction and a Few $S_{\text{N}}2$ Reactions of $X^- + \text{CH}_3Y \rightarrow \text{CH}_3X + Y^-$

X	Y	E_{col} (kcal/mol)	E_{rxn}^a (kcal/mol)	σ (\AA^2)	b_{max} (\AA)	$f_{\text{rel}}(\text{Ind})$	ref
OH	I	11.5	−62.1	16.5 ± 4.3	6.5	0.18 ± 0.02	35
		23.0		10.9 ± 3.1	6.0	0.15 ± 0.02	
F	I	7.4	−46.7	108.7 ± 9.7	8.8	0.21 ± 0.02	13
		35.2^b		8.6 ± 2.2^b	5.8^b	0.31 ± 0.02^b	
		35.2^c	−41.2	1.8 ± 0.3^c	4.8^c	0.15 ± 0.07^c	
Cl	I	9.0	−12.2	0.48 ± 0.26	4.0	^d	37
		17.5		0.31 ± 0.14	2.0	0.08 ± 0.05	
		19.6		7.2 ± 1.8	5.0	0.33 ± 0.11	
$\text{HBr}^+ + \text{CO}_2$		8.1	−0.3	11.7 ± 2.6	6.0	0.44 ± 0.05	
		19.6		7.2 ± 1.8	5.0	0.33 ± 0.11	

^aReaction energy without zero-point energy. ^bThe *ab initio* method employed in this AIMD simulation is B97-1/ECP/d. ^cThe *ab initio* method employed in this AIMD simulation is MP2/ECP/d. ^dThere is only one Ind trajectory.

The $X^- + \text{CH}_3\text{Y} \rightarrow \text{CH}_3\text{X} + \text{Y}^-$ type $\text{S}_{\text{N}}2$ reactions and the $\text{HBr}^+ + \text{CO}_2 \rightarrow \text{HOCO}^+ + \text{Br}$ reaction share common characteristics: backward scattering ($\theta > 90^\circ$) for DR, forward scattering ($\theta < 90^\circ$) for DS, and isotropic scattering for Ind.^{13,35–37,39} Nevertheless, the detailed differences in the scattering angle of direct reactive trajectories (i.e., DR and DS) suggest a potential impact of the mass of the reactant ion: the HBr^+ ion accounts for about two-thirds of the total mass of the system, while the reactant ion makes up only 20% of the total mass at most for the listed $\text{S}_{\text{N}}2$ reactions ($\text{Cl}^- + \text{CH}_3\text{I}$).³⁷ The heavier reactant ion has decreased the scattering angle of DR trajectories. For example, the $\text{HBr}^+ + \text{CO}_2$ reaction shows a narrowly distributed and close-to-vertical distribution of scattering angles, while trajectories of the same mechanism of $\text{S}_{\text{N}}2$ reactions show a distribution of scattering angles centered around 135° .^{13,35–37,39} However, the heavier reactant ion seems to have a negligible impact on the DS mechanisms as both $\text{HBr}^+ + \text{CO}_2$ and $\text{S}_{\text{N}}2$ reactions show distributions of scattering angles that are further away from 90° and much broader. It remains unclear why DR and DS respond differently to the increase in mass of the reactant ion, and further investigations of similar reactions are necessary.

As shown in Table 1, the trajectories of the Ind mechanism of $\text{HBr}^+ + \text{CO}_2$ become less elastic (i.e., preserve less relative translational energy) when the collision energy of the reactants increases. This result contradicts the premise that higher collision energies induce more elastic collisions. This premise, though simple, remains largely true for various $\text{S}_{\text{N}}2$ reactions listed in Table 2; for example, the relative translational energy of the product for the $\text{F}^- + \text{CH}_3\text{I} \rightarrow \text{CH}_3\text{F} + \text{I}^-$ reaction increased from 21 to 31% when E_{col} increased from 7.4 to 35.2 kcal/mol.¹³ This premise even holds true for $\text{S}_{\text{N}}2$ reactions of tertiary amines as well: for example, the relative translational energy of the product for the $\text{F}^- + \text{NH}_2\text{Cl} \rightarrow \text{NH}_2\text{F} + \text{Cl}^-$ reaction increased from 26 to 33% when E_{col} increased from 0.9 to 40.0 kcal/mol.³⁹ In some other cases of the $\text{S}_{\text{N}}2$ reactions, the relative translational energy of the product is slightly suppressed by the collision energy. For example, the relative translational energy of the product of $\text{OH}^- + \text{CH}_3\text{I} \rightarrow \text{CH}_3\text{Cl} + \text{I}^-$ decreases from 18 to 15% when the collision energy was doubled from 11.5 to 23.0 kcal/mol.³⁵ To the best of our knowledge, this is the first time that a relatively significant negative correlation between the collision energy and the fraction of translational energy of the products has been reported for an ion–molecular reaction. To unravel the counterintuitive results, the dependence of the relative translational energy of the products on the impact parameter b has been analyzed and the results are shown in Figure S2 in the Supporting Information. The relative translational energies of the products of Ind mechanism increase with the increase of b for both collision energies (the Pearson correlation coefficients for $E_{\text{col}} = 8.1$ kcal/mol and $E_{\text{col}} = 19.6$ kcal/mol are 0.62 and 0.75, respectively); thus, the Ind trajectories at larger b are expected to have higher relative translational energies. As mentioned in the manuscript, the Ind trajectories of $b \geq 2.0$ Å are largely absent at $E_{\text{col}} = 19.6$ kcal/mol; hence, the average relative translational energy of Ind is smaller compared to $E_{\text{col}} = 8.1$ kcal/mol, which includes many Ind trajectories of $b \geq 2.0$ Å.

In summary, this manuscript has revealed three reaction mechanisms contributing to the $\text{HBr}^+ + \text{CO}_2 \rightarrow \text{HOCO}^+ + \text{Br}$ reaction with AIMD simulations. The cross sections computed at two different collision energies, 8.1 and 19.6 kcal/mol, agree

well with the experimental observations. Analysis of the AIMD trajectories has shown nonintuitive behavior of the relative translational energy of the product in response to an increase of collision energy. Further investigations are necessary to explain the potential impact of massive reactant ions on ion–molecule reactions. This research has also laid a solid foundation to study how the rotational excitation of HBr^+ can affect the dynamics of the reaction in future work.

■ ASSOCIATED CONTENT

Supporting Information

The Supporting Information is available free of charge at <https://pubs.acs.org/doi/10.1021/acs.jpca.0c05323>.

A representative trajectory of the DR mechanism (Animation 1) (MPG)

A representative trajectory of the DS mechanism (Animation 2) (MPG)

A representative trajectory of the Ind mechanism (Animation 3) (MPG)

Summary of the AIMD simulations (Table S1); collision probability vs impact parameters (Figure S1); and correlation between $f_{\text{rel}}(\text{Ind})$ and b (Figure S2) (PDF)

■ AUTHOR INFORMATION

Corresponding Author

Rui Sun – Department of Chemistry, The University of Hawai'i at Manoa, Honolulu, Hawaii 96822, United States;
orcid.org/0000-0003-0638-1353; Email: ruisun@hawaii.edu

Authors

Yuheng Luo – Department of Chemistry, The University of Hawai'i at Manoa, Honolulu, Hawaii 96822, United States;
orcid.org/0000-0002-3124-1179

Kazuomi Fujioka – Department of Chemistry, The University of Hawai'i at Manoa, Honolulu, Hawaii 96822, United States

Alyson Shoji – Department of Chemistry, The University of Hawai'i at Manoa, Honolulu, Hawaii 96822, United States

William L. Hase – Department of Chemistry and Biochemistry, Texas Tech University, Lubbock, Texas 79409, United States;
orcid.org/0000-0002-0560-5100

Karl-Michael Weitzel – Fachbereich Chemie, Physikalische Chemie, Philipps Universität Marburg, 35037 Marburg, Germany; orcid.org/0000-0002-1560-235X

Complete contact information is available at:
<https://pubs.acs.org/doi/10.1021/acs.jpca.0c05323>

Notes

The authors declare no competing financial interest.

^{||}Dr. William L. Hase passed away on Mar 23rd, 2020.

■ ACKNOWLEDGMENTS

We thank the Information Technology Service (ITS) Cyberinfrastructure from the University of Hawai'i, Manoa, and XSEDE for the computational resources. We are grateful for the financial support from the University of Hawai'i, Manoa. Parts of this work have been supported by a grant from the Deutsche Forschungsgemeinschaft (We 1330-11).

■ REFERENCES

(1) Steinfeld, J. I.; Francisco, J. S.; Hase, W. L. *Chemical Kinetics and Dynamics*; Prentice Hall, 1999.

- (2) Pratihari, S.; Ma, X.; Homayoon, Z.; Barnes, G. L.; Hase, W. L. Direct Chemical Dynamics Simulations. *J. Am. Chem. Soc.* **2017**, *139*, 3570–3590.
- (3) Yang, X.; Clary, D. C.; Neumark, D. M. Chemical Reaction Dynamics. *Chem. Soc. Rev.* **2017**, *46*, 7481–7482.
- (4) Lee, Y. T. Molecular Beam Studies of Elementary Photophysical Processes. *Science* **1987**, *236*, 793–798.
- (5) Paetow, L.; Unger, F.; Beichel, W.; Frenking, G.; Weitzel, K. M. Rotational Dependence of the Proton-Transfer Reaction $\text{HBr}^+ + \text{CO}_2 \rightarrow \text{HOCO}^+ + \text{Br}$. I. Energy versus Angular Momentum Effects. *J. Chem. Phys.* **2010**, *132*, 174305.
- (6) Paetow, L.; Unger, F.; Beutel, B.; Weitzel, K. M. Rotational Dependence of the Proton-Transfer Reaction $\text{HBr}^+ + \text{CO}_2 \rightarrow \text{HOCO}^+ + \text{Br}$. II. Comparison of $\text{HBr}^+ (2\Pi_{1/2})$ and $\text{HBr}^+ (2\Pi_{3/2})$. *J. Chem. Phys.* **2010**, *133*, 234301.
- (7) Uhlemann, T.; Wallauer, J.; Weitzel, K. M. Self-Reactions in the $\text{HCl}^+ (\text{DCl}^+) + \text{HCl}$ System: A State-Selective Investigation of the Role of Rotation. *Phys. Chem. Chem. Phys.* **2015**, *17*, 16454–16461.
- (8) Pariser, R.; Parr, R. G. A Semi-Empirical Theory of the Electronic Spectra and Electronic Structure of Complex Unsaturated Molecules. I. *J. Chem. Phys.* **1953**, *21*, 466–471.
- (9) Parr, R. G.; Craig, D. P.; Ross, I. G. Molecular Orbital Calculations of the Lower Excited Electronic Levels of Benzene, Configuration Interaction Included. *J. Chem. Phys.* **1950**, *18*, 1561–1563.
- (10) Sun, R.; Granucci, G.; Paul, A. K.; Siebert, M.; Liang, H. J.; Cheong, G.; Hase, W. L.; Persico, M. Potential Energy Surfaces for the $\text{HBr}^+ + \text{CO}_2 \rightarrow \text{Br} + \text{HOCO}^+$ Reaction in the $\text{HBr}^+ 2\Pi_{3/2}$ and $2\Pi_{1/2}$ Spin-Orbit States. *J. Chem. Phys.* **2015**, *142*, 104302.
- (11) Shoji, A.; Schanzenbach, D.; Merrill, R.; Zhang, J.; Yang, L.; Sun, R. Theoretical Study of the Potential Energy Profile of the $\text{HBr}^+ + \text{CO}_2 \rightarrow \text{HOCO}^+ + \text{Br}$ Reaction. *J. Phys. Chem. A* **2019**, *123*, 9791–9799.
- (12) Mikosch, J.; Trippel, S.; Eichhorn, C.; Otto, R.; Lourderaj, U.; Zhang, J. X.; Hase, W. L.; Weidemüller, M.; Wester, R. Imaging Nucleophilic Substitution Dynamics. *Science* **2008**, *319*, 183–186.
- (13) Mikosch, J.; Zhang, J.; Trippel, S.; Eichhorn, C.; Otto, R.; Sun, R.; De Jong, W. A.; Weidemüller, M.; Hase, W. L.; Wester, R. Indirect Dynamics in a Highly Exoergic Substitution Reaction. *J. Am. Chem. Soc.* **2013**, *135*, 4250–4259.
- (14) Xie, J.; Hase, W. L. Rethinking the SN_2 Reaction. *Science* **2016**, *352*, 32–33.
- (15) Hase, W. L.; Buckowski, D. G.; Swamy, K. N. Dynamics of Ethyl Radical Decomposition. 3. Effect of Chemical Activation vs Microcanonical Sampling. *J. Phys. Chem. A* **1983**, *87*, 2754–2763.
- (16) López, J. G.; Vayner, G.; Lourderaj, U.; Addepalli, S. V.; Kato, S.; DeJong, W. A.; Windus, T. L.; Hase, W. L. A Direct Dynamics Trajectory Study of $\text{F} + \text{CH}_3\text{OOH}$ Reactive Collisions Reveals a Major Non-IRC Reaction Path. *J. Am. Chem. Soc.* **2007**, *129*, 9976–9985.
- (17) Yu, F. Ab Initio Direct Classical Trajectory Investigation on the S N_2 Reaction of F^- with NH_2F : Nonstatistical Central Barrier Recrossing Dynamics. *J. Comput. Chem.* **2012**, *33*, 401–405.
- (18) Pritchard, H. O. Recrossings and Transition-State Theory. *J. Phys. Chem. A* **2005**, *109*, 1400–1404.
- (19) Komatsuzaki, T.; Nagaoka, M. Study on “Regularity” of Barrier Recrossing Motion. *J. Chem. Phys.* **1996**, *105*, 10838–10848.
- (20) Tuckerman, M. E. Ab Initio Molecular Dynamics: Basic Concepts, Current Trends and Novel Applications. *J. Phys.: Condens. Matter* **2002**, *14*, R1297–R1355.
- (21) Raghavachari, K.; Trucks, G. W.; Pople, J. A.; Head-Gordon, M. A Fifth-Order Perturbation Comparison of Electron Correlation Theories. *Chem. Phys. Lett.* **1989**, *157*, 479–483.
- (22) Peterson, K. A.; Woon, D. E.; Dunning, T. H. Benchmark Calculations with Correlated Molecular Wave Functions. IV. The Classical Barrier Height of the $\text{H} + \text{H}_2 \rightarrow \text{H}_2 + \text{H}$ Reaction. *J. Chem. Phys.* **1994**, *100*, 7410–7415.
- (23) Varandas, A. J. C. Basis-Set Extrapolation of the Correlation Energy. *J. Chem. Phys.* **2000**, *113*, 8880–8887.
- (24) Parr, R. G. Density Functional Theory of Atoms and Molecules. In *Horizons of Quantum Chemistry*; Fukui, K.; Pullman, B., Eds.; Springer Netherlands: Dordrecht, 1980; pp 5–15.
- (25) Møller, C.; Plesset, M. S. Note on an Approximation Treatment for Many-Electron Systems. *Phys. Rev.* **1934**, *46*, 618–622.
- (26) Szabo, A.; Ostlund, N. S. *Modern Quantum Chemistry: Introduction to Advanced Electronic Structure Theory*; Dover Publications: New York, 1996.
- (27) Dolg, M.; Cao, X. Relativistic Pseudopotentials: Their Development and Scope of Applications. *Chem. Rev.* **2012**, *112*, 403–480.
- (28) Dunning, T. H. Gaussian Basis Sets for Use in Correlated Molecular Calculations. I. The Atoms Boron through Neon and Hydrogen. *J. Chem. Phys.* **1989**, *90*, 1007–1023.
- (29) Peterson, K. A.; Figgen, D.; Goll, E.; Stoll, H.; Dolg, M. Systematically Convergent Basis Sets with Relativistic Pseudopotentials. II. Small-Core Pseudopotentials and Correlation Consistent Basis Sets for the Post-d Group 16 – 18 Elements Systematically Convergent Basis Sets with Relativistic Pseudopotentials. *J. Chem. Phys.* **2003**, *119*, 11113–11123.
- (30) Yamamoto, N.; Vreven, T.; Robb, M. A.; Frisch, M. J.; Bernhard Schlegel, H. A Direct Derivative MC-SCF Procedure. *Chem. Phys. Lett.* **1996**, *250*, 373–378.
- (31) Hu, X.; Hase, W. L.; Pirraglia, T. Vectorization of the General Monte Carlo Classical Trajectory Program VENUS. *J. Comput. Chem.* **1991**, *12*, 1014–1024.
- (32) Valiev, M.; Bylaska, E. J.; Govind, N.; Kowalski, K.; Straatsma, T. P.; Van Dam, H. J. J.; Wang, D.; Nieplocha, J.; Apra, E.; Windus, T. L.; De Jong, W. A. NWChem: A Comprehensive and Scalable Open-Source Solution for Large Scale Molecular Simulations. *Comput. Phys. Commun.* **2010**, *181*, 1477–1489.
- (33) Lourderaj, U.; Sun, R.; Kohale, S. C.; Barnes, G. L.; De Jong, W. A.; Windus, T. L.; Hase, W. L. The VENUS/NWChem Software Package. Tight Coupling between Chemical Dynamics Simulations and Electronic Structure Theory. *Comput. Phys. Commun.* **2014**, *185*, 1074–1080.
- (34) Paranjothy, M.; Sun, R.; Zhuang, Y.; Hase, W. L. Direct Chemical Dynamics Simulations: Coupling of Classical and Quasiclassical Trajectories with Electronic Structure Theory. *Wiley Interdiscip. Rev.: Comput. Mol. Sci.* **2013**, *3*, 296–316.
- (35) Xie, J.; Sun, R.; Siebert, M. R.; Otto, R.; Wester, R.; Hase, W. L. Direct Dynamics Simulations of the Product Channels and Atomistic Mechanisms for the $\text{OH}^- + \text{CH}_3\text{I}$ Reaction. Comparison with Experiment. *J. Phys. Chem. A* **2013**, *117*, 7162–7178.
- (36) Sun, R.; Davda, C. J.; Zhang, J.; Hase, W. L. Comparison of Direct Dynamics Simulations with Different Electronic Structure Methods. $\text{F} + \text{CH}_3\text{I}$ with MP2 and DFT/B97-1. *Phys. Chem. Chem. Phys.* **2015**, *17*, 2589–2597.
- (37) Zhang, J.; Lourderaj, U.; Sun, R.; Mikosch, J.; Wester, R.; Hase, W. L. Simulation Studies of the $\text{Cl}^- + \text{CH}_3\text{I}$ SN_2 Nucleophilic Substitution Reaction: Comparison with Ion Imaging Experiments. *J. Chem. Phys.* **2013**, *138*, No. 114309.
- (38) Zhang, J.; Hase, W. L. Electronic Structure Theory Study of the $\text{F}^- + \text{CH}_3\text{I} \rightarrow \text{FCH}_3 + \text{I}^-$ Potential Energy Surface. *J. Phys. Chem. A* **2010**, *114*, 9635–9643.
- (39) Liu, X.; Zhao, C.; Yang, L.; Zhang, J.; Sun, R. Indirect Dynamics in $\text{SN}_2@N$: Insight into the Influence of Central Atoms. *Phys. Chem. Chem. Phys.* **2017**, *19*, 22691–22699.
- (40) Sun, R.; Xie, J.; Zhang, J.; Hase, W. L. The $\text{F}^- + \text{CH}_3\text{I} \rightarrow \text{FCH}_3 + \text{I}^-$ Entrance Channel Potential Energy Surface Comparison of Electronic Structure Methods. *Int. J. Mass Spectrom.* **2015**, *377*, 222–227.
- (41) Becke, A. D. A New Mixing of Hartree–Fock and Local Density-functional Theories. *J. Chem. Phys.* **1993**, *98*, 1372–1377.